A Double-Cross Linking Approach for High Fidelity 3D-Printing of Cell-Laden Scaffolds for Bone Regeneration

Ahmer Shehzad, Bachelor of Science

Submitted in fulfillment of the requirements
for the degree of Master of Science

in Biomedical Engineering

NAZARBAYEV
UNIVERSITY

School of Engineering and Digital Sciences
Department of Chemical and Materials Engineering

Nazarbayev University

53 Kabanbay Batyr Avenue,
Nur-Sultan, Kazakhstan, 010000

Supervisor: Prof. Dana Akilbekova, Prof. Cevat Erisken

DECLARATION

I hereby, declare that this manuscript, entitled "*A Double-Cross Linking Approach for High Fidelity 3D-Printing of Cell-Laden Scaffolds for Bone Regeneration*" is the result of my own work except for quotations and citations, which have been duly acknowledged. I also declare that, to the best of my knowledge and belief, it has not been previously or concurrently submitted, in whole or in part, for any other degree ordiploma at Nazarbayev University or any other national or international institution.

Name: Ahmer Shehzad

Date: April 28, 2022

Abstract

Introduction: Artificial organ development, especially bone, is considered a challenging and complicated procedure in tissue engineering, which finds its application in eliminating animal trials and alternative ways to overcome the scarcity of organ donors and avoid host transplant rejection. Bone injury recovery mechanisms are usually longer and more complicated. Traditional clinical treatments such as bone grafts are considered nowadays for efficient recovery mechanisms. However, host rejection and infection proliferation resulted in an unsatisfactory recovery mechanism. Biopolymers are highly biocompatible and have tunable mechanical properties for bone regeneration applications. Biomaterials provide the interconnected porous structure that mimics the native bio-environment, governs the extracellular matrix, and facilitates bone tissue formation. Optimization of shear thinning properties contributes to the fabrication of high-fidelity scaffolds via extrusion-based bioprinting. A high-fidelity scaffold promotes cell proliferation and cues extracellular matrix, which corresponds to aligned collagen fiber.

Method: Here, we proposed various blends of hydrogel composite such as %Algiante/%Gelatin/%GelMA ranges from I (1/4/5), II (1/8/2.5), and III (1/2/10), respectively, to produce high fidelity mesenchymal stem cell-laden scaffold with excellent cell viability, characterized by rheological analysis, scanning electron microscopy(SEM), nuclear magnetic resonance(NMR) spectroscopy and confocal microscopy respectively. The double crosslinking approach was utilized , i.e., ionic crosslinking of alginate polymer with calcium ions and covalent bonding between GelMA chains mediated by UV irradiation in the presence of LAP photoinitiator, provided strong mechanical properties which enhance the biodegradability.

Result: The scaffold obtained with various porosity and pore sizes ranges from 50 to 120 µm and high printing accuracy up to 95%, which promoted cell adhesion, proliferation, and migration, and facilitated cell differentiation and tissue development. The scaffold with a low concentration of GelMA ranging from 2.5 to 5 % demonstrated high cell viability and Alkaline Phosphatase (ALP) activity, demonstrating the presence of osteocytes. Alizarin Red, H&E, and Masson Trichrome staining depict calcium deposition, extracellular matrix, and collagen fiber.

Conclusion: Based on the excellent cytocombaitbility and proliferation rates, the reported hydrogel construct will be used in the development in *vitro* bone organoids. These scaffold model not only useful for bone regeneration but also finds its application in other tissue engineering application.

Acknowledgments

I would like to express my sincere gratitude and appreciation to all those who have supported me throughout this research project and helped me in the completion of this thesis.

First and foremost, I would like to thank my thesis supervisor Prof. Dana Akilbekova, for her guidance, support, and invaluable insights throughout this project. Her constant encouragement and feedback helped me to stay motivated and focused throughout the research process.

I would also like to extend my thanks to my co supervisor Prof. Cevat Erisken, who served on my thesis committee. Their constructive feedback and suggestions were instrumental in shaping my research and in making this thesis a success.

My heartfelt thanks go to my family for their love, support, and encouragement throughout my academic journey. Their unwavering belief in me has been a constant source of inspiration and motivation.

I would like to express my appreciation to my friends who have supported me during my graduate studies. Their encouragement and support have made the journey more enjoyable and memorable.

Finally, I would like to thank all the participants who generously gave their time and contributed to this study. Without their willingness to participate, this research would not have been possible.

Once again, thank you to everyone who has supported me throughout this project. Your support has been invaluable, and I am grateful for all that you have done.

Table of Contents

List of Abbreviations

GelMA	Gelatin Methacrylate
Alg	Alginate
Gel	Gelatin
LAP	Lithium phenyl (2,4,6-trimethylbenzoyl) phosphinate
ALP	Alkaline phosphatase
H & E	Hematoxylin and Eosin
PBS	Phosphate Buffered Saline
MSCs	Mesenchymal stem cells
$CaCl_2$	Calcium Chloride
UV	Ultraviolet
I	1% Alg/4% Gel/5% GelMA
II	1% Alg/8% Gel/2.5% GelMA
III	1% Alg/2% Gel/10% GelMA

List of Figures and Tables

Chapter 1_Indroduction

Bone tissue is an important component of the vertebrate skeleton, providing strong support for the body and protecting crucial organs. It also serves as a reservoir for important ions such as calcium and phosphate, which can be distributed or kept in a controlled manner to ensure optimum concentration levels in body fluids. While bone growth, also known as osteogenesis, occurs via two basic bony processes (intra-articular and intra-chondral), the former produces woven bone, which is quickly replaced by more robust lamellar bone[1]. Bone is a complex tissue made up of various elements such as organic and mineral elements, highly specialised cell types, and water. The formation of bone occurs in two stages, beginning with the formation and secretion of the extracellular matrix (also known as osteoid) and ending with mineralization. The ECM is mostly made up of type I collagen (about 90%), as well as other proteins like non-collagenous proteins, glycosaminoglycans, and growth factors. The mineral component of bone is hydroxyapatite, which is formed when inorganic phosphate and calcium ions (Ca2+) combine. Osteoblasts, which are derived from mesenchymal stromal cells, are the cells responsible for bone formation (MSCs)[2].

Natural bone's remarkable mechanical properties are closely related to its hierarchical structure that spans the nano- to macro-scales, as well as its precisely organized inorganic and organic components at the nanoscale. As shown in Figure 1, hydroxyapatite (HA) nanocrystals are periodically deposited within the collagenous gap regions during bone biomineralization. Natural bone has two distinct structures: the exterior (compact bone), which is made up of Haversian canals and osteons, and the interior (spongy bone), which is made up of trabecular structures with porosities ranging from 75% to 85%. The extracellular matrix (ECM) of natural bone contains four types of cells: osteoblasts, osteoclasts, osteocytes, and bone lining cells[3, 4].

Osteoblasts are active osteoblasts that synthesize and mineralize new bone matrix as well as repair older bone, whereas osteocytes are dormant osteoblasts that become trapped within the mineralized bone matrix. The matrix is absorbed by osteoclasts, and bone lining cells are dormant cells that can differentiate into osteoblasts[5]. These cells play an important role in bone metabolism and maintain a balanced state during dynamic bone remodeling. Furthermore, several cytokines, including insulin-like growth factors, platelet-derived growth factors, fibroblast growth factors, vascular endothelial growth factors (VEGFs), transforming growth factors, and bone

morphogenic proteins (BMPs), are sequestered within the bone matrix, where they regulate bone metabolism, function, and regeneration[6-8].

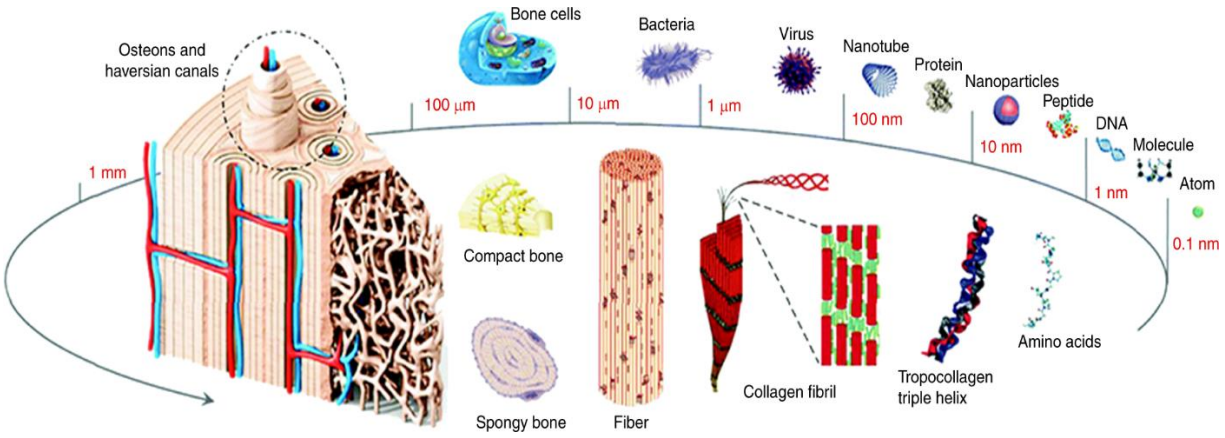

Figure 1. Bone structural and physiological hierarchy[9]

Several drawbacks are associated with using allografts or autografts to restore bone structure and function. These drawbacks include rejection due to immune reactions, infection, or a lack of supply. To address these limitations, scientists have developed synthetic bone grafts made of various biomaterials, including natural or synthetic polymers, metallic composites, or ceramics[10-12]. **Figure 1** illustrates the hierarchical structure of bone, which consists of a macroscopic structure of compact and spongy bone, the composition of compact bone, collagen fibrils that make up the lamellar structure of bone osteons, tropocollagen molecules formed by triple amino acid chains, and hydroxyapatite crystals[13-15]. However, mimicking the complex tissue architecture and biomechanical function of bone is a significant hurdle. Thus, new engineering strategies, such as 3D bioprinting, hold great promise for producing constructs that replicate the anatomical features of native bone tissue.

Bioprinting has emerged as a promising technique for bone regeneration due to its ability to precisely control the architecture and composition of 3D constructs. The optimal scaffold design for bone regeneration should mimic the natural extracellular matrix (ECM) of bone tissue and support cell proliferation, differentiation, and mineralization[16]. One key advantage of bioprinting is the ability to create scaffolds with interconnected pores and channels, which can promote nutrient and waste exchange and facilitate the formation of new bone tissue. Additionally, bioprinting allows for the incorporation of bioactive molecules and growth factors into the scaffold, which can further enhance bone regeneration. To achieve successful bone regeneration

using bioprinting, several factors must be considered, including the choice of bioink, the printing parameters, and the post-printing processing steps. The bioink should be biocompatible and support cell viability and differentiation, while the printing parameters should be optimized to ensure accurate deposition and scaffold architecture. Post-printing processing steps, such as crosslinking and cell seeding, can further enhance scaffold properties and promote bone regeneration [12, 17, 18].

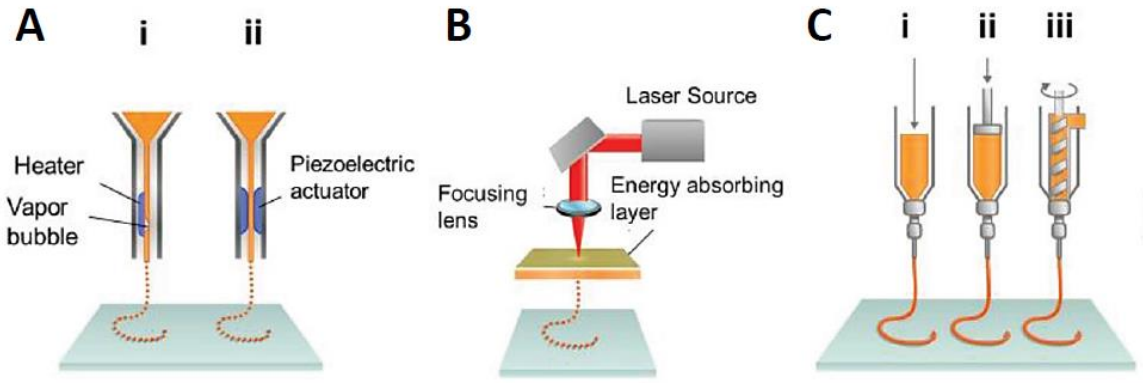

Figure 2. Various bioprinting methodologies, **A)** Inkjet bioprinitng , **B)** Laser-aided bioprinting and , **C)** Extrusion bioprinting[19]

Furthermore, to achieve tissue formation successfully, the degradation rate of scaffold must corresponds to rate of formation of new tissue without compromising the required mechanical stability. To achieve the required criteria, it is important to comprehend the various 3D bioprinting methods and biomaterial behavior along with physiochemical features during and after printing procedure[20]. Bioprinting is divided into three basic approaches, namely inkjet, extrusion, and laser aided bioprinting **Figure 2**, based on the procedures used to discharge biomaterials from the orifice. Inkjet bioprinting either thermally or piezoeletrocally deposits biomaterials through the nozzle as layered construct. A structure formed by the accumulation of tiny droplets caused by pressure vibration, which can be achieved using a heater or piezoelectric crystals. In laser assisted bioprinting, a highly powerful laser pulse is employed to generate high pressure, resulting in the evacuation of bioink from the reservoir into the platform as predesign construct. Extrusion bioprinting is the dispensing of hydrogel either pneumatically or mechanically extruded using plastic syringes loaded with bioink on the receiving stage, either by piston or screw based assembly[21-23]. Bioprinting technologies have advanced the biofabrication mechanism;

nonetheless, the gelation features of bioink pose challenges, both physically and biologically, in achieving high fidelity bioprinted scaffolds with cytocompatible abilities. The rheological characteristics of the hydrogel and its crosslinking methods plays a major role in bioprinting mechanism. However, the printing parameters such as temperature adjustment, printing speed, and extrusion pressure and nozzle diameter dictate the fabrication of tissue constructed through bioprinting procedures. The rheological characteristics of the hydrogel determines the shear thinning and gelation behaviors, when applied external pressure during bioprinting[24, 25]. Additionally, the amount polymer, its molecular weight and viscosity of bioinks, plays crucial role in determining the shear stress required during biopinting to achieve mechanically stable construct[26]. High shape fidelity of the tissue construct achieved with the increase in the concentration of polymer, however, the proliferation rate of cells compromises due to the increase in the extrusion pressure during bioprinting process[27]. The shear thinning characteristics of the biomaterials facilitates in the hydrogel deposition on the receiving platform as with the increase in the shear rate , the viscosity decrease due to the redistribution of the polymers chains when applied pressure[28]. Gelation of bioink is compulsory to hold the shape of the scaffold after printing. There are two major categories of the gelation process, either physical or chemical crosslinking mechanism[29]. Physical crosslinking is the entrapment of polymer chain, by ionic, hydrophobic interaction or hydrogen bonding. Furthermore, physical crosslinking approaches are applied due to their biocompatibility and reversible abilities, and however, they exhibit poor mechanical stability. To modify mechanical properties, irreversible crosslinking approach are designed to add chemical functional groups that crosslinking the hydrogel composite via covalent bonding[30]. Chemical crosslinking mechanisms, increased the mechanical characteristics of hydrogel and irreversibility, that hold the construct after printing either by photo polymerization or enzyme based crosslinking[31] **Figure 3**. In scaffold design, physiochemical and biological characteristics of hydrogel can be shaped by controlling the bioprinting process, the composition of biomaterials and the crosslinking approach. For optimal bone formation, bioprinting process faced a lot of challenges such as bioink compositions, bioactive molecules and crosslinking approaches[32]. The bioinks are formed by the combination of natural or synthetic biomaterials such as collagen, alginate, gelatin, chitosan, fibrin, PCL, PVA, PEG, etc. Natural polymers demonstrated good cytocompatible abilities with strong mechanical properties required for the formation of extracellular matrix. They also boost tissue formation by promoting cell proliferation and

adhesion. Moreover, scaffold degraded with corresponding to new tissue formation by either metabolic or enzymatic reactions[33, 34]. Alginate is the natural polymer that frequently used in the tissue engineering applications due its viscosity, gelation, and biocompatible properties.

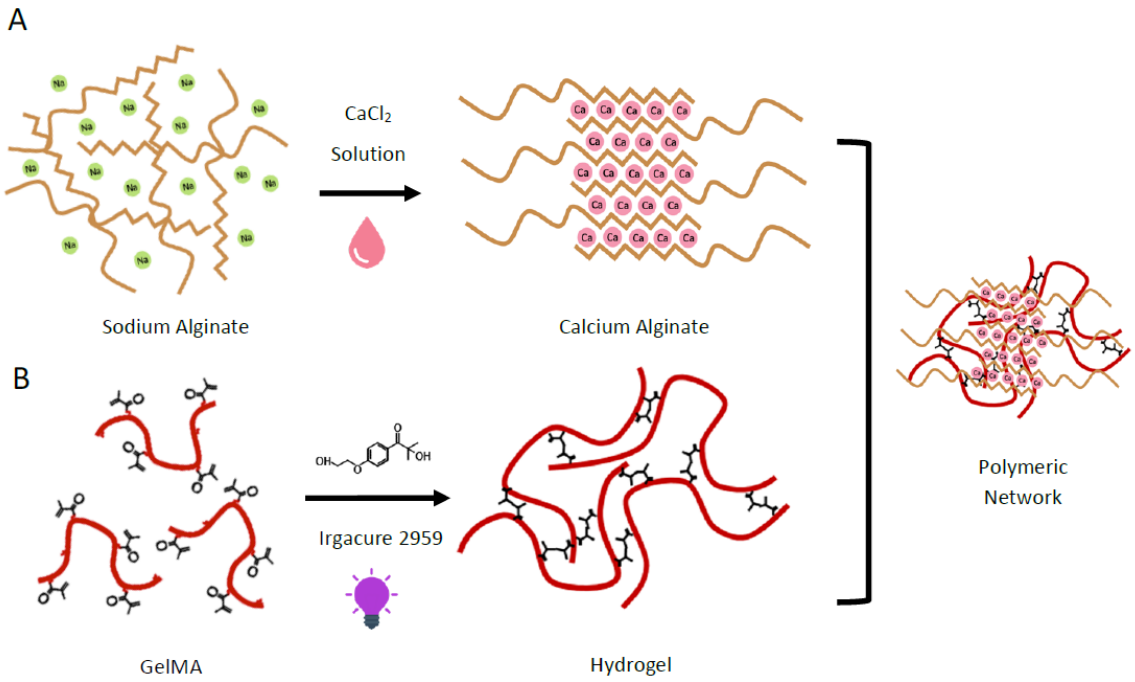

Figure 3. Dual crosslinking techniques **A)** Demonstration ionic crosslinking of alginate polymer with calcium ions bridging, and B**)** GelMA covalent crosslinking in presence of UV irradiation and photo initiator[35]

The mechanical properties of alginate hydrogels can be improved by the addition of calcium chloride solution, which creates the ionic bonds between the calcium ions and polymeric chains resulted in an ionic crosslinking mesh. However, due to not enough mechanical characteristics and biological activity of alginate, various polymers such as gelatin, chitosan, collagen etc. was added to fabricate the stronger hydrogel. Gelatin is extensively used in bone tissue engineering applications due to its high shear thinning and thermo-responsive properties. Additionally, its morphological and physiological characteristics are quite similar to collagen, the major component in bone and extracellular matrix. Combining both gelatin and alginate, the fast gelation mechanism of alginate and high shear-thinning, thermo-responsive gelatin, resulted into achieving high fidelity with stronger mechanical properties. Additionally, gelatin facilities proliferation, differentiation

and cell adhesion[36, 37]. However, gelatin has low mechanical stability and faster degradation kinetics in aqueous medium such as PBS and culture media. Although gelatin can be chemically modified, by functionalizing it with methylation process, exchanging gelatin amino groups with methacryloyl groups, resulted into gelatin methacryloyl (GelMA) that is photopolymerizable in the presence of photo-initiator under UV irradiation. To achieve more thickly polymeric mesh, dual crosslinking technique can be used, by combining Ca_{2+} ions mediated ionic crosslinking with UV-initiated chemical crosslinking in GelMA[38, 39]. Histological analysis of the bioprinted construct is important in determining the bone formation mechanism, especially the composition of biomaterials and their crosslinking mechanism. Although, histological analysis determined the structure biological content at microscopic level, however, colorimetric analysis provide the association between the individual components. Alizarin Red S is the most common histological method to visualize the mineralization of bioprinted tissue construct. Moreover, H & E staining is used for the visualization of cell nucleus and extracellular matrix[40-43].

1.1 Aims and Objectives

The bone model presented in this research project will provide improved biodegradability, cell proliferation, and migration, facilitating the initiation of ECM components and assisting in the development of collagen matrix formation. High-fidelity scaffolds with robust mechanical properties will be achieved using various compositions of bioinks comprising gelatin methacryloyl (GelMA), alginate, and gelatin with mouse mesenchymal stem cells. The stability and printability of the constructs will be controlled via two approaches: 1. Optimization of precursor's ratio and concentration, and 2. Via dual crosslinking mechanism of photoinitiated covalent bonding and ionic Ca^{2+}-assisted stabilization.

1.2 Thesis Statement

In bone regeneration, the success of the bone-implant interface highly depends on the ECM which cues the formation of bone fibers. To evaluate biocompatibility and bone regeneration effects such as osteoinduction and osteoconduction of the implants, traditional in-vitro methods do not account for the native ECM microenvironment. To confirm the actual human bone in-vivo environment, a bone organoid model that establishes the approximate physiology of human bone is necessary. Hopefully, with these bone-in-vitro models, the success rate in bone defect treatments

and prosthetic surgeries will increase significantly. Several attempts have recently been made to construct a bone in-vitro model, with relatively limited success. To create a viable bone model, proper physiochemical and scaffold architecture are essential to induce ECM that promotes cell mineralization. Meanwhile, the scaffold should degrade with the formation of new tissue to ensure optimal mechanical functionality [17, 44, 45]. In this work, a 3D bioprinter will be used to create a human 3-D organotypic bone model. The 3D bioprinting technique will be used to create a polymeric scaffold by incorporating primary human cells directly in the bioink [10].

1.3 Hypothesis

The ability of the bioink to be printable and have advantageous physical properties as shear thinning while also maintaining its structure after printing in the culture is necessary for high-fidelity 3-D printing of cell-containing scaffolds. Here, a double-crosslinking approach (ionic and covalent) for the 3-D printing of alginate and gelatin-based bioink with photo-responsive mechanical properties is proposed. Co-printing bioinks with various polymer compositions with distinct degradation rates that will enable the construction of a scaffold with optimal mechanical functionality [10, 46].

1.4 Literature Review

Due of its high gelation and adjustable stiffness qualities, alginate is commonly employed in extrusion-based bioprinting. Alginate is highly biocompatible, and its degradation kinetics can be controlled using calcium ions-assisted cross-linking. [47, 48]. Gelatin, on the other hand, is a well-known polymer in the field of bone regeneration due to its thermo-responsive properties and similar structure to collagen. Because of its poor viscoelastic qualities, gelatin is quite biodegradable. The biodegradability of gelatin can be modified by adding methroyloyl groups in exchange for gelatin amine groups resulting in gelatin methacryloyl (GelMA) [49-53]. The bioink consists of a photoinitiator such as LAP or igracure that helps in the photoinitiated cross-linking at 365 nm UV irradiation [54, 55]. The denser interconnected porous structure can be achieved by the introduction of the double crosslinking through the combination of chemical bonded photo-induced crosslinking of GelMA and calcium ions-mediated alginate ionic crosslinking [39, 56]. Additionally, gelatin is added to GelMA can increase its thermo-rheological characteristics. Yin *et al.* demonstrated high cell viability and printing fidelity with a 5%/8% Gelatin/GelMA hydrogel composite. However, failed to retain scaffold integrity required for osteogenic differentiation and

extracellular matrix formation after printing with bone mesenchymal stem cell.[57]. In one of the studies, Tabriz *et al*. demonstrated the printing of alginate polymers with human brain tumor cells with 88% cell viability up to 11 days. However, a sharp decline in cell viability was observed after 11 days [58]. Wust *et al.* constructed a scaffold composed of 2% w/v alginate and 10% w/v gelatin, achieving 85% of cell viability after 3 days. However, one disadvantage is that it must be kept in calcium chloride-containing cell culture medium to prevent degradation [59]. Presently, there is no adequate *in-vitro* model that can mimic the physiological characteristics of human bone to demonstrate the remolding process in bone regeneration to produce a 3D *in vitro* bone model for tissue-engineered organized bone [60-66]

The current research involves using the previously mentioned techniques to examine how human mesenchymal stem cells differentiate into osteoblast and demonstrate mineralization and ECM formation in 3D bioprinted scaffold. Additionally, three different bioinks will be compared to see how they affect the formation of extracellular matrix (ECM). The goal of the project is to establish a method for visualizing and characterizing ECM formation with the bone mineralization in the scaffold matrix. To achieve this, 3D bioprinting technology will be utilized to create polymeric scaffolds layer by layer. Colorimetric assays and histological methods will be employed to evaluate the quality and organization of the ECM and bone mineralization.

Chapter 2_Methodology

2.1 Material

Gelatin from porcine skin (strength 300. Type A), sodium alginate (99% purity), lithium phenyl-2,4,6-trimenthylbenzoylphosphinate (LAP), methacrylic anhydride (MA), Sodium bicarbonate, phosphate-buffered saline (PBS), calcium chloride, live/dead viability assay kit, and cell culture reagents (Fetal bovine serum (FBS), 0.25% Trypsin EDTA, Dulbecco's Modified Eagle Medium (DMEM), antibiotic antimycotic solution) were purchased from Sigma-Aldrich. NIH/3T3 cell line (from the American Type Cell Collection, ATCC® CRL-1658TM), Rat Mesenchymal Stem Cells (Sigma Aldrich), Hematoxylin (Sigma Aldrich), Eosin(Sigma Aldrich), Alizarin Red S (Sigma Aldrich), Poly-L-lysine Sigma-Aldrich (Sigma Aldrich),

2.2 Equipment

Scanning Electron microscopy SEM (JSM-IT200 (LA)

Rheometer (Anton Paar MCR 302)

Incubator (BINDER GmbH)

Safety cabinet (ESCO NordicSafe Microbiological Safety Cabinets Class II)

Confocal laser scanning microscope LSM 780 (Zeiss)

Leica DM750 Clinical Microscope

Lyotrap freeze dryer

BIO X Bioprinter (CELLINK)

Mechanical testing Machine

Cryotome (Thermo fisher scientific)

UV LAMP

1H NMR spectrometry (JNM-ECA 500, Japan)

MestreNova NMR software (version 6.0.2, Mestrelabs Research)

2.3 GelMA Synthesis and Bioink preparation

The GelMA was produced by the reaction of methacrylate anhydrate with gelatin as reported in the protocol[67]. Briefly, 20 g of gelatin was added in the 200 ml of PBS at 50 °C on the magnetic stirrer for 30 minutes until it completely dissolved to obtain 10 % (w/v) gelatin. Then 10 % (w/v) methacylate anhydrate was added drop wise to achieved high degree of functionalization of gelatin methacrylate (GelMA) and stirred for 3 hours at 50 °C. The unreacted methacrylate was eliminated by centrifugation at 3500g for 5 minutes and the supernatant was goes through dilution by two folds in PBS. The diluted GelMA was filled in dialysis membrane (12-14 kDa) and put to dialysis for 7 days in deionized water to completely remove the untreated methacrylate anhydrate. After dialysis, the pH was normalize to 7.4 by adding 3 N sodium hydroxide. The GelMA solution was freeze-dried and stored in -20 ^{o}C. For preparation of bioink prior to bioprinting , different composition of gelatin (2-8) w/v %, GelMA (2.5 -10) w/v % , 1% of alginate were dissolved in PBS by heating it for 15 minutes at 45℃ and added 0.5 w/v % LAP photoinitator in the dissolved composite. The composite polymers were heated again for 15 minutes at 45℃ to get three composition of ink named I.II, III.

2.4 Rheological Characterization of Hydrogel

To observe the viscoelastic and mechanical properties of the hydrogel composition, rheological analysis was performed by the rheometer. To determine the gelation point of hydrogel, the storage modulus G’ and loss storage modulus G’ was calculated in the temperature range between 10 to 40 ℃ with the inclination rate of 1℃/min at the constant shear stain (γ) 1% and frequency 1 Hz.

Moreover, the rotation test was conducted at 15 ℃ to observe the relationship between viscosity and shear rate. The flow rate was maintained between 0.1 and 100 per second during the flow curve exam. For both oscillatory and rotation test, 50 mm cone parallel plate geometry was used. The relationship between temperature and viscosity was also observed in oscillatory analysis.

2.5 3D bioprinting of bioink formulation

The inks were prepared one day before printed and filtered with 0.45 µm syringe filter. The good printing conditions were maintained with the help of BIO X 3D bioprinter. All scaffold were printed using the temperature regulated printhead to ensure the bioprinting of the construct in a

favorable environment. The temperature was regulated between 18-22 ℃ depending upon the composition of the bioink utilized. Before printing, the inks were pasteurized at 50℃ and form homogenous mixture by continuously infilling and outfilling (10 times) of ink in a falcan tube, the ink was filtered through the syringe filter (0.22 micron) and transferred in a 5 ml eppendroff tube. The 15 million cells were added in the 3ml filtered ink to make the composition of hydrogel 5 million cells per ml. The bioink, then mixed with 300 microliter of culture media and transferred in the printer extruder and place in ice for various time range between (0.33-2) minutes depending upon concentration of gelatin and GelMA in bioink I, II, III. The bioink was extruded layer by layer deposition on the printing platform through the needle while maintaining the temperature between 21 to 23 ℃. The uniform speed of 5 mm/s was kept constant to smoothly print the scaffold. The scaffold was fabricated by applying the pressure on the extruder in the range of 45-90 kPA through the fixed 27G gauge needle depending upon the hydrogel composition.

Table 1. Bioink composition of the 3D printed scaffold

Ink Composition	**Alginate (mg/ml)**	**Gelatin (mg/ml)**	**GelMA (mg/ml)**	**PBS (ml)**
I (1% Alg/4% Gel/5% GelMA)	100	400	500	8
II (1% Alg/8% Gel/2.5% GelMA)	100	800	250	8
III (1% Alg/2% Gel/10% GelMA)	100	200	1000	8

The printed scaffold was first irradiated upto 20 seconds under UV radiation (365 nm) for GelMA chemical crosslinking and then transferred the scaffold in 2% w/v calcium chloride solution for 10 minutes for alginate ionic crosslinking. After crosslinking, scaffold were washed thrice in culture media to remove extra unbounded calcium ions and transferred in the well plates containing control medium and put in incubator for 37 ℃.

2.6 Characterization of internal morphology of the scaffold

To observe the internal morphological structure of scaffold, the scaffold were first freeze-dried and then applied gold sputtering up to 7 nm to prepare for Scanning Electron microscopy SEM imaging analysis. The setting of 10 kv accelerating voltage with 58 C current was used to observe the scaffold morphology.

2.7 Swelling and Degradation kinetics of hydrogel

The swelling capacity of the scaffold was observed over the passage of time in PBS and the swollen weights of the scaffold were measured consequently up to 14 days. Three scaffold of each composition of hydrogel were submerged into the phosphate buffer saline and put in the incubator at 37° C and 5% CO_2 and their weights measured at fixed time points of 1 h, 5 h for each scaffold. The weight of the freeze-dried scaffold and their swollen weights, after carefully blotted with Kim wipes to remove excess water were measured after 1 h and 5 h in PBS solution.

$$\text{Swelling capacity \% (SC)} = \frac{W(t)-W(0)}{W(0)} \text{ x } 100\% \qquad (1)$$

where W(t) is the scaffold's weight after each incubation time interval and W(0) is the dry weight of the scaffold.

2.8 Degradation kinematics of the scaffold

To observe the degree of degradation with the passage of fixed points, the freeze dried scaffold were placed in culture media and incubated for 14 days in the incubator at fixed condition at 5% CO_2 and 37° C while measuring the weight of the scaffold in two days gap interval ranging from day 1 to day 14. The initial (freeze-dried) and final weight (after freeze-dried after immersing in culture media) were measured and the degradation kinetics were determined with the following equation:

$$\text{Degradation degree \% (DD)} = \frac{W(0)-W(f)}{W(0)} \text{ x}100\% \qquad (2)$$

Where W (f) was the final freeze dried weight and W (0) was the initial weight measured before degradation test.

2.9 Printing Accuracy of the scaffold

The printing accuracy was calculated with the difference between the measurement of the computer aided designed model and the printed scaffold. To determine the printing accuracy of the scaffold, the surface area of the constructed voids in the scaffold was preferred, which is the ratio of the sum of actual surface area of the printed scaffold and the sum of the surface area of the CAD model. Total 64 voids were selected for the measurement of the surface area of the printed scaffold and the printing fidelity was calculated with the help of the following equation

$$\text{Printing accuracy \% (PA)} = \frac{\sum A_{void}(\text{theoretical})}{\sum A_{void}(\text{practical})} \text{x}100\% \qquad (3)$$

For each composition, average data of three replicates were used with the precision of 4% variability in fidelity

2.10 GelMA characterization by NMR analysis

1H NMR spectroscopy was used to determine the degree of functionalization of GelMA[68]. In a nutshell, 1 ml of deuterium oxide D2O was mixed with 16 mg of GelMA and gelatin. And the solutions were transferred to NMR tubes and perform the 1H NMR for 256 cycles. The following equation is used to find the degree of functionalization was used:

$$DoF = \left(1 - \frac{LGelMA}{LGelatin}\right) * 100 \qquad (4)$$

where *L*GelMA and *L*Gelatin are integra area of the peaks of lysine signals of GelMA and gelatin.

The peaks of the spectra were quantified using MestreNova software. The amount of functionalization is defined as the ratio of methacrylate groups connected to amine lysine functional group in residual gelatin and GelMA

2.11 Cell culture for bioprinting:

The NIH/3T3 cell line (from the American Type Cell Collection, ATCC® CRL-1658TM) was grown in standard conditions containing DMEM, 10% FBS, and 1% penicillin/streptomycin and incubated at 37 °C with 5% CO2. 0.25% trypsin EDTA was employed during cell passage to remove cells. The mesenchymal stem cells were grown in DMEM with 10% FBS, 1% penicillin/streptomycin, 1% non-essential amino acids (NEAA), and one microliter bFGF aliquot. For both cell lines, passage seven was employed for cell-laden printing, with the culture media changed every three days. To convert mesenchymal stem cells into osteoblasts, osteogenic medium was produced by combining control media, a 50 g/ml ascorbic acid aliquot, 100 nM Dexamethasone, and 10 nM Beta-glycerophosphase.

2.12 Live/Dead staining for bioprinted scaffold

The viability of cells was assessed on day 3, 7 and day 14 using live/dead staining. To evaluate cell viability, calcein-AM (green fluorescence) was used to identify live cells, ethidium homodimer (red fluorescence) for dead cells, and Hoechst to stain all cells.

To perform the staining, the culture media was removed, and the scaffolds were incubated in staining media containing 2 μM calcein-AM, 4 μM ethidium homodimer, and 5 μg/mL Hoechst. The scaffolds were then covered in foil and incubated in an incubator at 37 ℃ and 5% CO2 for 40 minutes. After staining, the scaffolds were washed twice with phosphate buffer saline.

To observe cell viability, the scaffolds were imaged under a confocal microscope using a live cell incubation chamber. The excitation and emission were set to 404/517 nm for live cells and 517/617 nm for dead cells, respectively. Hoechst excitation and fluorescence were maintained at 350/461, respectively, to stain all cells. The images were captured with a 10x resolution and analyzed using ImageJ software.

2.13 Osteogenic Differentiation assessment by ALP ElSA

The osteogenic differentiation of the bioprinted scaffold was observed by detecting alkaline phosphatase activity with the Abcam ALP test kit (ab83369). At 37°C and 5% CO2, the scaffolds were placed in an incubator with osteogenic differentiation media. The alkaline phosphatase activity was assessed at regular intervals over 42 days by collecting the osteogenic media and measuring the activity at 405 nm absorbance with a microplate reader. The ALP activity was determined by comparing the sample's optical density (OD) to that of the blank, using a standard curve prepared from an ALP standard solution (0-10 ng/ml).

2.14 Hematoxylin and Eosin Staining

To begin, the scaffold was rinsed with a solution containing calcium chloride and sodium chloride to fixate it. Then, it was treated with a fixative called paraformaldehyde and left at room temperature for 2 hours. After fixation, the scaffold was soaked in solutions containing sucrose at varying concentrations for 16 hours at room temperature. The scaffold was then frozen in liquid nitrogen and cut into thin slices using a process called cryosectioning. To visualize the structure of the scaffold, the cryosections were stained with a combination of hematoxylin and eosin. The

hematoxylin stains the nuclei of the cells in the scaffold, while the eosin stains the extracellular matrix and other cellular components. The scaffold section was first immersed in hematoxylin for 1 minute and then rinsed with tap water. Next, it was stained with eosin for 1 minute and again rinsed with distilled water. To remove excess dye, the scaffold section was then dehydrated using a series of washes in ethanol, xylene, and acetone. Finally, the scaffold section was mounted onto a glass slide using DPX mounting medium and observed under a microscope. The images were captured and analyzed using ImageJ software.

2.15 Measurement of Mineralization in scaffold by Alizarin Red Staining

To assess the level of calcification in the bioprinted scaffold, a specific method was used. A solution of Alizarin Red S, which was dissolved in distilled water with a pH level of 4.2 and had a concentration of 2% (w/v), was applied to the scaffold for one minute. After several washes in distilled water and dehydration procedures as outlined in the H&E staining process, the glass slides were prepared with DPX medium. The stained slides were then examined under a Leica microscope, and photographs were taken.

Chapter 3_ Result and Discussion

3.1 Bioink formulation and viscoelastic characteristics of the Alginate/Gelatin/GelMA scaffold

Bioink Formulation is the important for achieving high fidelity scaffold with high mechanical characteristics. In our research, three potential compositions of Algiante/Gelatin/GelMA as mention in Table 1, were considered due to their high shear thinning and printable properties. The three compositions were marked as the I (1%/4%/5%), II(1%/8%/2.5%), and III (1%/2%/10%) to demonstrate various compositions of Algiante/Gelatin/GelMA. These composition of biomaterials were selected because of their suitability for 3D bioprinting and high biocompatibility with low toxicity. The gelatin and GelMA were the main biomaterial that grant mechanical stability and shape fidelity after the chemical crosslinking. On the other hand, alginate additional material that provide extra stability through ionic crosslinking and also facilitates cell proliferation. During initial scrutiny for potential biomaterial selection, it was observed the more than 1% (w/v) alginate does not facilitates in further scaffold stability while decreasing the printability of the scaffold. Therefore, fixed concentration of alginate was used while regulating the bioprinting via GelMA and gelatin concentration. The GelMA and its degree of functionalization was measured by NMR, confirming the presence of methyl groups as identified peaks between 5.3 to 5.6 ppm in the spectrum **(Figure S1)**. In current research, the various concentration of gelatin and GelMA was selected as mention before to observe the cell growth and tissue formation. Addition of gelatin enhances the shear thinning properties and improve shape fidelity.

The study systematically investigated the rheological behaviors of various inks at different temperatures and shear rate ranges. The gelation point was determined by analyzing the storage and loss moduli (G' and G") and viscosity changes at relevant temperatures. The hydrogel compositions exhibited a typical hydrogel behavior, with noticeable elastic behavior below the gelation temperature. **Figure 4A** displays the viscoelastic properties of hydrogel formulations, with arrows indicating the gelation points. The gelation point of Composition I and III was observed at 25 ^{o}C, while Composition II was at 30 ^{o}C due to a higher content of gelatin.

Figures 4 B, C show the viscosity of the hydroges at various shear rates and temperatures. Shear thinning was observed in all formulations as the viscosity decreased with increasing shear rate and temperature, leading to uniform extrusion of all bioinks during bioprinting. Composition II had a higher viscosity than the other two inks (I and III), suggesting higher shape fidelity and finer filament deposition but potentially lower cell survival. The optimal printing conditions were achieved at sub-solution/gel transition temperature (25 ^{o} C), at a low shear rate, to avoid cell damage while maintaining printing accuracy and post-production shape fidelity. The results indicate that the rheological properties of bioinks can be tailored for specific printing requirements by adjusting the composition, temperature, and shear rate.

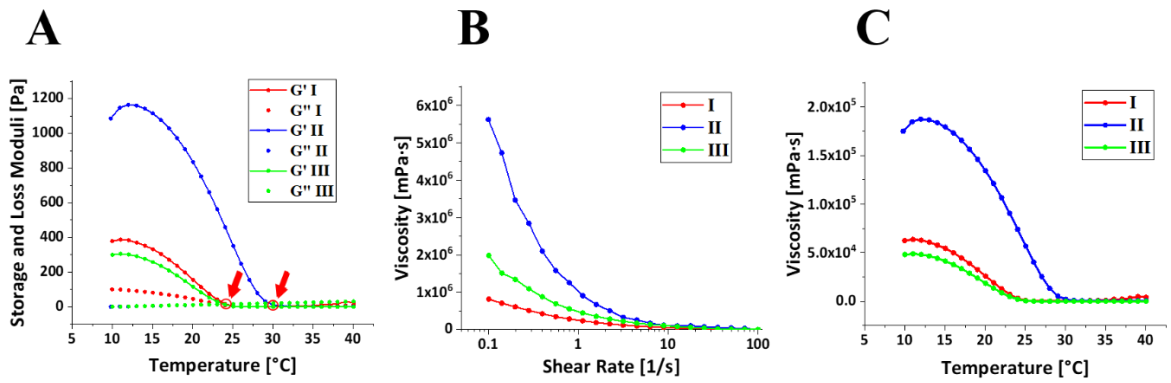

Figure 4. Rheological characterization of various (Alginate/Gelatin/GelMA) bioink compositions: I (1/4/5), II(1/8/2.5), III(1/2/10) in values of % w/v**. (A)** Storage (G') and Loss (G") moduli vs. temperature. Gelation points are indicated with arrows, **(B)** Viscosity vs. shear rate and **(C)** Viscosity vs. temperature.

3.2 Fabrication and morphological properties of 3D bioprinted scaffolds.

As shown in **Figure 5**, the selected ink formulations were loaded with mesenchymal stem cells and were bioprinted, and immediately cured under 365 nm UV irradiations for 20 seconds, and then crosslink by calcium ions bridging of CaCl2 containing culture medium to allow covalent and ionic crosslinking.

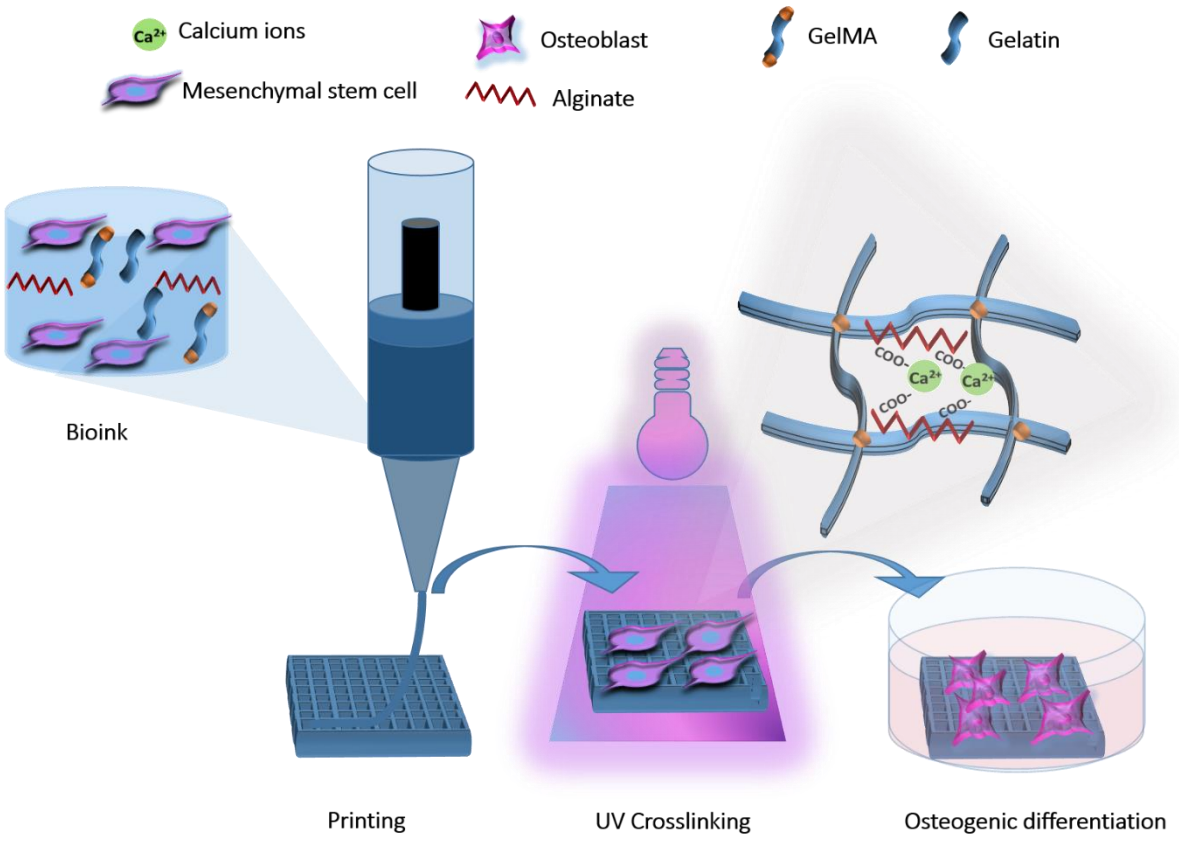

Figure 5. Fabrication procedure of Alg/Gelatin/GelMA bioprinted scaffold

In **Figure 6A**, images of the 15-layer 3D-printed scaffolds made from different inks are shown. The accuracy of the printing is shown in the small images within the larger pictures, with values of 85%, 93%, and 74% for biomaterial formulations I, II, and III, respectively. Gelatin has superior properties that make it more suitable for printing, and ink composition II, which has the highest gelatin content, had the highest printing accuracy and shape fidelity over time. While ink III has higher viscosity at low shear rates due to its higher GelMA concentration, the accuracy and shape fidelity of the printed scaffolds depend more on the amount of gelatin in the formulation.

The SEM images, demonstrated in **Figures 6B**, **C**, and **D**, are referred to the top, cross-sectional, and magnification images, respectively, demonstrating macro porous and interconnected network of hydrogel for all 3D printed scaffolds, fabricated from the respective ink formulations.

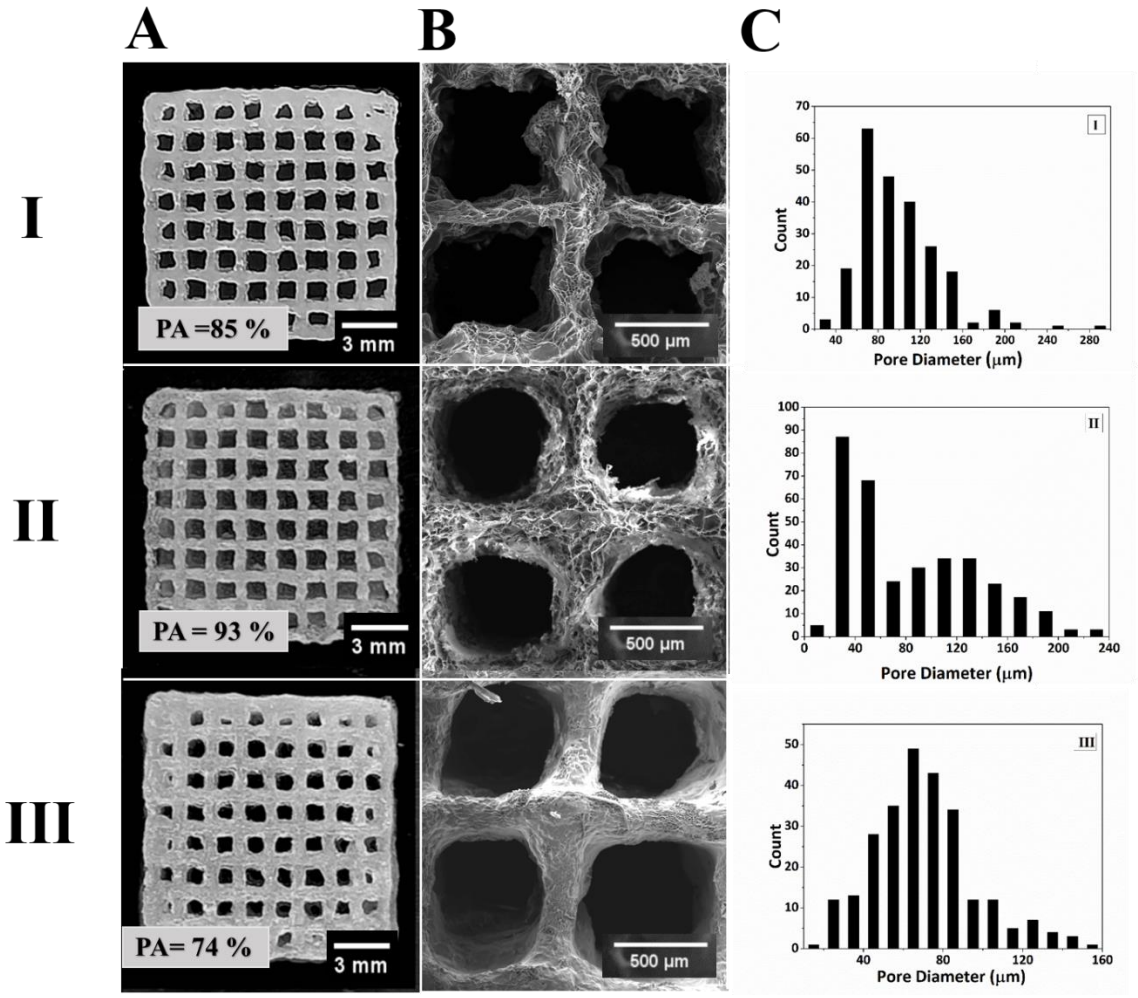

Figure 6. Photographs and obtained SEM images of the different formulations (%Alginate/%Gelatin/%GelMA), I (1/4/5), II (1/8/2.5), III (1/2//10%), **(A)** Photographs of scaffolds post printing along with printing accuracy, and SEM images, **(B)** top view, **(C)** Pore size distribution of the I, II, and III formulations

The **Figure 6C** displays the distribution of pore sizes in the 3D-printed scaffolds. The results showed that Scaffold I, which was made using ink compositions I and III, had a single type of pore size ranging from 40 to 230 µm. The average pore size for composition I was 99 µm and for composition III, it was between 20 to 160 µm. On the other hand, Scaffold II exhibited a bimodal pore size distribution with two distinct types of pore sizes. The larger pores had a size range of 10 to 230 µm, and the smaller pores branched off from these larger ones. The highest proportions of pore sizes were observed at around 60 µm and 125 µm.The difference in pore size distribution between the scaffolds was attributed to the ink composition, which is influenced by the

concentration and proportion of Gel/GelMA components, crosslinking functionalities, and ink viscosity. The study found that higher concentrations of polymers or crosslinking agents resulted in reduced pore size and increased pore density. Inks with a balanced Gel/GelMA ratio and low viscosity produced a uniform distribution of pore sizes. For instance, ink composition I resulted in a monomodal pore size distribution with a Gaussian profile. In contrast, Scaffold II had a bimodal pore size distribution due to a high Gel content in the ink, which resulted in a high viscosity that hindered diffusion and caused an inhomogeneous distribution of methacrylate. Scaffold III, on the other hand, had a monomodal pore size distribution despite its comparatively low viscosity. This was due to a high GelMA ratio and high total polymer concentration in the ink.

3.3 Physical and Mechanical properties of bioprinted scaffolds

The produced scaffolds were assessed for their physical and mechanical properties, including swelling capacity, degradation rate, and stress/strain behavior. **Figure 7A** illustrates the swelling capacity of the scaffolds after 1 and 5 hours. Scaffold II exhibited the highest swelling capacity, with about 900% after one hour and 1213 ± 9% after 5 hours. This is consistent with the observed bimodal pore distribution, where larger pores initially swell followed by smaller cavities. Scaffold II has a lower content of GelMA, which is responsible for the covalent hydrogel crosslinking, and a higher Gel ratio, which provides the primary building material. This high polymer concentration allows for the entanglement of water molecules within the scaffold matrix, while lower crosslinking density contributes to the thinning of the scaffold walls. In contrast, Scaffold I had a smaller swelling capacity of approximately 600% after one hour, with a slight increase to 653 ± 5% after 5 hours. This corresponds to the ink composition, which has higher GelMA and lower Gel content, resulting in a porous morphology with a unimodal size distribution profile and a larger average pore diameter. Scaffold III had a limited swelling capacity of only 580 ±10%, which remained unchanged after one hour.

Both Ink I and Ink III share similar mechanical stability factors such as polymer concentration and crosslinking density, which contribute to smaller intermolecular distances and porosity. However, Ink I (653 ± 5%) had a slightly higher swelling capacity than Ink III (580 ± 10%) due to a higher crosslinking density resulting from an increase in GelMA concentration from 5% to 10%. The varying concentrations of biopolymer and crosslinking densities influenced the structural stability and pore volume capacity of the scaffold, leading to differences in water

absorption. Ink I and III demonstrated a capillary effect that allowed for rapid water saturation inside the scaffold pore mesh, resulting in no significant difference between 1-hour and 5-hour swelling. However, Ink II showed a significant difference in water uptake due to the availability of more polymer content within the internal mesh, enabling the entanglement of water molecules and weaker intermolecular forces from lower concentrations of crosslinking densities.

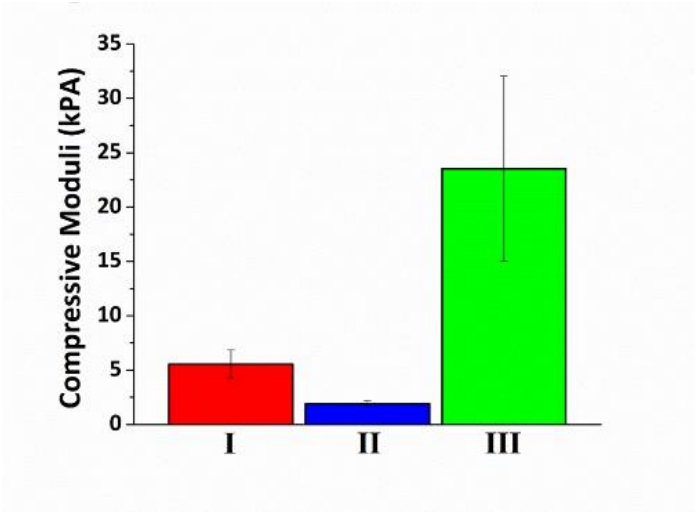

Figure 7. Compressive moduli of the scaffolds obtained from the respective ink formulations (I, II, and III).

The data shows how the degradation rates changed over two weeks. Composition I degraded more slowly than Composition II because of the appropriate crosslinking density of GelMA. The rate of degradation ranged from 40.4 ± 12.3% (I) to 40.6 ± 12.9% (III) as the crosslinking density increased from 2.5% to 10%. A higher concentration of GelMA led to a slower degradation rate, confirming previous research [69]. On the other hand, Composition II (66.7 ± 12.4%) degraded faster than Compositions I and III due to its bi-model porosity arrangement and high swelling capacity. Water molecules rapidly degraded the scaffold, particularly in Composition II, by widening the pores through both capillary and hydrolysis activities. A faster degradation rate indicates a weaker structure, while a slower rate can interrupt cell proliferation and extracellular matrix accumulation[70]. All three compositions effectively promoted bone tissue regeneration with appropriate degradation rates. The scaffold's interconnected microporous structure affects its mechanical strength and breakdown dynamics [71].

To evaluate the mechanical properties of the hydrogel, a compression test was conducted. The results depicted in **Figure 7** indicated that Ink III had a higher compressive modulus of 24±8.5 kPA compared to Inks I and II due to its larger concentration of GelMA (10% w/v). The increased concentration of GelMA led to a higher crosslinking density, which resulted in better mechanical properties of the hydrogel. Maintaining the scaffold's integrity in culture media depends on the degree of crosslinking density, which also affects degradation and swelling kinetics. It's worth noting that the scaffold's long-term stability was achieved through dual crosslinking - alginate-ionic crosslinking and GelMA-covalent crosslinking. However, relying solely on a single crosslinking method significantly impacted the hydrogel's mechanical properties.

3.4 Cell viability and cell proliferation in the bioprinted scaffold

Efficient cell proliferation and successful scaffold colonization are vital for the integration of the scaffold and the formation of ECM[72]. The mechanical properties of the scaffold can affect cell behavior, as having optimal stiffness can improve cell survival over time and encourage the development of a 3D cellular network in printed scaffolds[64].

In this study, the viability and proliferation of MSCs after 3D bioprinting, and the effect of the scaffold on the survival of NIH/3T3 fibroblast cells were examined over 14 days of culturing in osteogenic media. The distribution and morphology of cells were qualitatively analyzed in scaffolds with different compositions. In **Figure 8**, the results showed that compositions I and II had a minimum viability of 96%, with no significant variation in viable cells over time. However, on days 3 (89.81.9), 7, and 14, composition III exhibited a substantial reduction in its cell survivability relative to compositions I and II. The 10% reduced cell viability in the bioink is apparently due to greater compressive stresses during bioprinting, which induced cell membrane rupture[73].

In the viscoelastic state (10°C), the elastic modulus of composition III with higher GelMA concentration was significantly higher than that of the bioinks with lower GelMA. The zoomed images showed that most cells in composition III retained a spherical morphology, while cells in compositions I and II exhibited a spreading morphology. Overall, the study suggested that cell bioprinting was highly effective in compositions with a lower concentration of GelMA, and scaffolds from compositions I and II supported normal cellular metabolic function for several weeks.

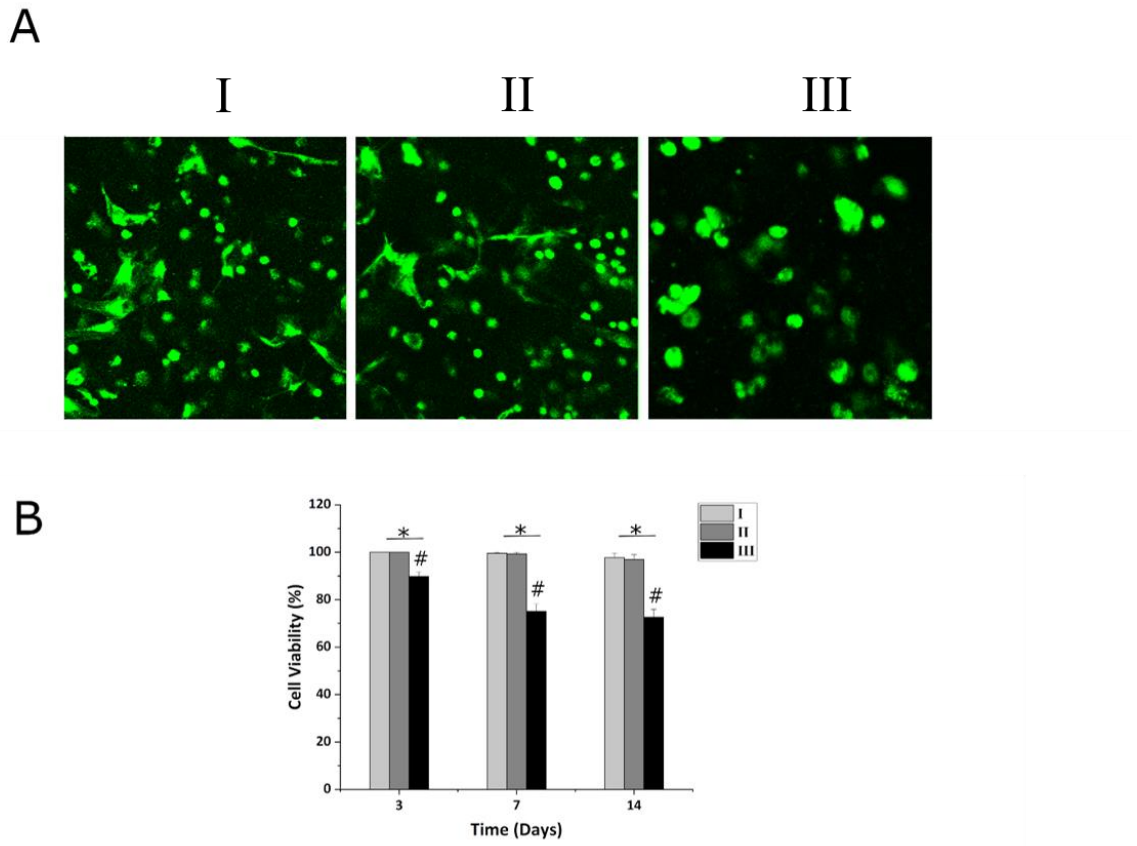

Figure 8. Live/Dead Cell viability, **A)** Live/Dead staining ,where green florescence corresponds to live cells and zoom in confocal images representing cell alignment and behavior at day 14, **B)** Live and Dead cells measurements corresponds to cell viability in percentages

3.5 Analysis of osteogenic differentiation by ALP ELISA

The study aimed to investigate the process of transforming MSCs into osteogenic cells by analyzing the concentration of ALP in the serum. To achieve this, the ALP activity of MSCs of the bioprinted scaffold was measured over a period of six weeks. The results, presented in **Figure 9A**, showed that the ALP activity increased in all compositions as the weeks passed. However, during weeks 3, 5, and 6, there was a marked increase in ALP activity in scaffold I, which contained cells, in comparison to the other cell-laden scaffolds with compositions II and III. The latter scaffold experienced a slight increase in ALP activity until week 4, and no notable change was observed for the remaining weeks. Composition II did not show any significant change in ALP activity over the six weeks. Overall, the findings indicate that scaffold I is more effective in

promoting the differentiation of MSCs into osteogenic cells, which is a promising outcome for bone tissue engineering applications.

3.6 Histological staining for Bone ECM development and Mineralization

The study examined the creation and mineralization of bone extracellular matrix (ECM) in 3D bioprinted scaffolds, which were analyzed through histology after being cultured for six weeks in osteogenic media. The results in **Figure 9B** demonstrated that composition I, which contained cells, exhibited a stronger red color intensity with Alizarin Red S staining than the other compositions, indicating a higher mineral content. Composition III did not display any color, suggesting no mineral content. H&E staining showed that compositions I and II had a uniform cell distribution throughout the scaffold, whereas composition III had a non-uniform distribution, with staining mainly located in the middle between the scaffold's voids. Figure 4 displayed the cell morphology on day 42, revealing the connection between cell morphology and ECM and mineral formation. The softer scaffolds (compositions I and II) had a higher cell density and cell spreading morphology was more noticeable in them than the stiff composition III scaffold.

The study aimed to explore the impact of scaffold stiffness on cell viability and morphology, as well as ALP activity. Researchers conducted experiments using cell-laden scaffolds with varying levels of stiffness and observed their behavior over time. The findings indicated that after 14 days, cells in softer scaffolds exhibited greater viability and spreading morphology compared to those in firmer ones. Furthermore, the Tanmay Jain *et al.* revealed[74] that bioinks with lower GelMA density facilitated better mass transfer, cell migration, and growth in softer environments compared to those with higher GelMA density. These results align with prior research on cell proliferation in 3D-printed hydrogels with different compressive moduli, which found that higher stiffness levels led to reduced viability and impaired nutrient diffusion rates. Over time, the viability of cells in the firmer scaffolds also decreased in culture media.

Previous research has demonstrated that the osteogenic differentiation and ALP activity of MSCs increase when cultured on stiffer 2D substrates[75]. However, in 3D environments, stiffer materials can impede cell proliferation and spreading, which could potentially reduce the potential for osteogenic differentiation. The images of cells in **Figure 9B** and support this by showing that cells in soft scaffolds have better spreading morphology, which may expedite MSCs' osteogenic differentiation and promote ECM formation and mineralization. Additionally, histology revealed

that 3D bioriented soft scaffolds had a greater degree of mineral formation compared to their stiffer scaffold counterparts, as seen in **Figure 9B**. These results align with findings from previous studies in the literature[64].

Apart from the physical properties of scaffolds, the microstructure of hydrogel scaffolds can also significantly affect cell culture outcomes. This microstructure can change due to variations in the concentration of GelMA, a material commonly used in hydrogel scaffolds. Increasing the concentration of GelMA results in a higher degree of crosslinking, which causes the polymer chains to become denser and decreases the number of small pores in the scaffold. This decrease in micro-porosity can adversely affect the delivery of nutrients and normal cellular functions.

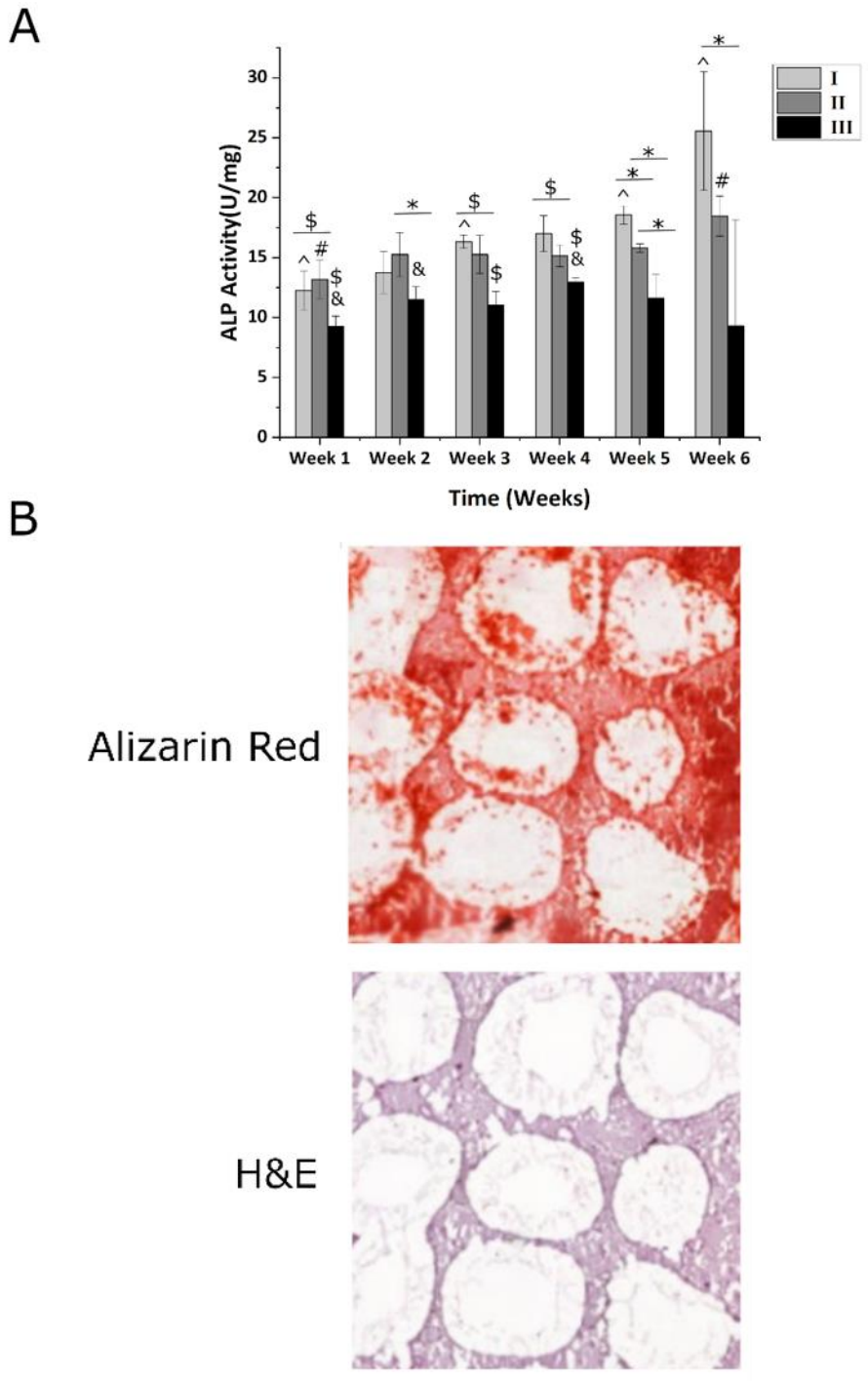

Figure 9. ALP activity and histological stainings for ECM formation and bone mineralization, **A)** Alkaline phosphatase activity demonstrating mineralization trends over the period of six weeks, **B)** Hematoxylin and Eosin, Alizarin Red , demonstrating ECM formation with bone mineralization within the 3D construct

Chapter 4 _ Conculsion

This study used various methods of staining and colorimatric assays to evaluate the presence of ECM and minearlization in the 3D bioprinted matrix ,fabricated from three different formultaions of biomaterials. The hydrogel construct described in this study has shown to have great cyto-compatibility and a high rate of cell proliferation. Due to these positive outcomes, the scaffold is being considered for use in the development of in vitro bone organoids.The scaffold model developed in this study has potential not only for bone regeneration, but also for other tissue engineering applications. Its versatility allows for its use in a variety of tissue engineering projects where a biocompatible and supportive scaffold is required for cell growth and tissue development.Overall, the results suggest that the hydrogel construct described in this study is a promising candidate for tissue engineering applications and may provide a valuable tool for researchers in this field.

Supplementary Documents

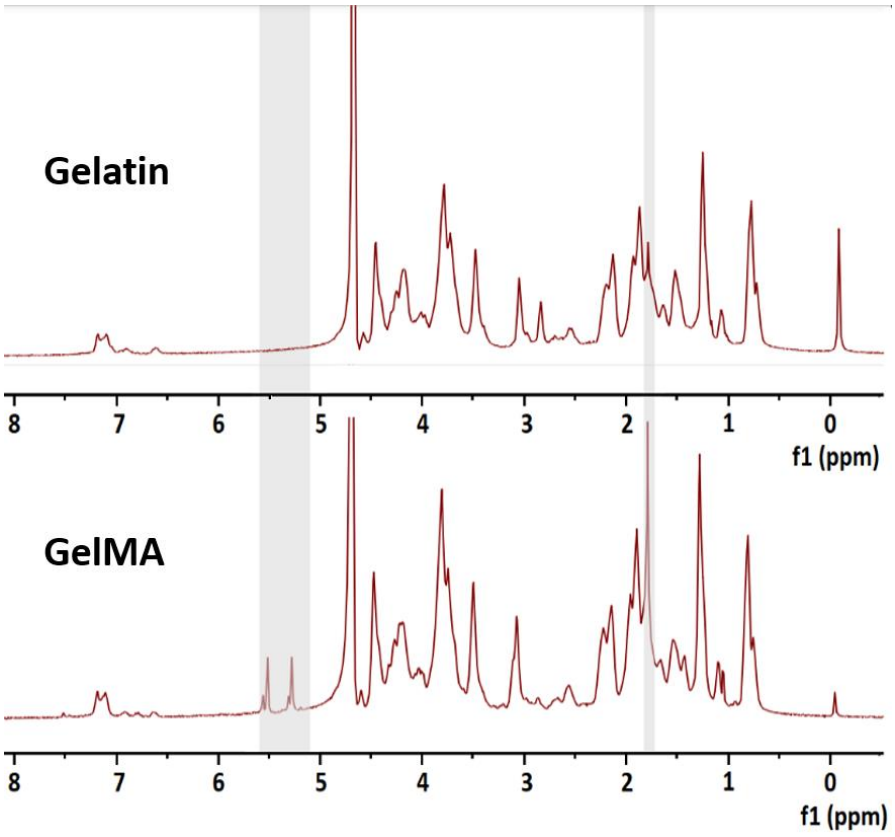

Figure S 1. Nuclear Magnetic Resonance (NMR) curve of GelMA and Gelatin

References

[1] A. Wawrzyniak and K. J. A. Balawender, "Structural and Metabolic Changes in Bone," vol. 12, no. 15, p. 1946, 2022.

[2] L. E. Bourne, C. P. Wheeler-Jones, and I. R. J. J. o. E. Orriss, "Regulation of mineralisation in bone and vascular tissue: A comparative review," vol. 248, no. 2, pp. R51-R65, 2021.

[3] Z. Liu, M. A. Meyers, Z. Zhang, and R. O. J. P. i. M. S. Ritchie, "Functional gradients and heterogeneities in biological materials: Design principles, functions, and bioinspired applications," vol. 88, pp. 467-498, 2017.

[4] A. V Singh and K. J. C. p. d. K Mehta, "Top-down versus bottom-up nanoengineering routes to design advanced oropharmacological products," vol. 22, no. 11, pp. 1534-1545, 2016.

[5] S. L. Dallas, M. Prideaux, and L. F. J. E. r. Bonewald, "The osteocyte: an endocrine cell… and more," vol. 34, no. 5, pp. 658-690, 2013.

[6] L. Zhu, D. Luo, and Y. J. I. J. o. O. S. Liu, "Effect of the nano/microscale structure of biomaterial scaffolds on bone regeneration," vol. 12, no. 1, p. 6, 2020.

[7] X. J. C. c. b. Feng, "Chemical and biochemical basis of cell-bone matrix interaction in health and disease," vol. 3, no. 2, pp. 189-196, 2009.

[8] S. Viguet-Carrin, P. Garnero, and P. J. O. i. Delmas, "The role of collagen in bone strength," vol. 17, pp. 319-336, 2006.

[9] Z. Fang, J. Chen, J. Pan, G. Liu, C. J. F. i. B. Zhao, and Biotechnology, "The development tendency of 3D-printed bioceramic scaffolds for applications ranging from bone tissue regeneration to bone tumor therapy," vol. 9, p. 754266, 2021.

[10] M. Hospodiuk, M. Dey, D. Sosnoski, and I. T. J. B. a. Ozbolat, "The bioink: A comprehensive review on bioprintable materials," vol. 35, no. 2, pp. 217-239, 2017.

[11] S. Das *et al.*, "Bioprintable, cell-laden silk fibroin–gelatin hydrogel supporting multilineage differentiation of stem cells for fabrication of three-dimensional tissue constructs," vol. 11, pp. 233-246, 2015.

[12] N. Ashammakhi *et al.*, "Advancing frontiers in bone bioprinting," vol. 8, no. 7, p. 1801048, 2019.

[13] D. J. Hadjidakis and I. I. J. A. o. t. N. Y. a. o. s. Androulakis, "Bone remodeling," vol. 1092, no. 1, pp. 385-396, 2006.

[14] J. E. Shea and S. C. J. A. d. d. r. Miller, "Skeletal function and structure: implications for tissue-targeted therapeutics," vol. 57, no. 7, pp. 945-957, 2005.

[15] P. T. Leali *et al.*, "Bone fragility: current reviews and clinical features," vol. 6, no. 2, p. 109, 2009.

[16] R. Fattahi, F. M. Chamkhorami, N. Taghipour, S. H. J. T. Keshel, and Cell, "The effect of extracellular matrix remodeling on material-based strategies for bone regeneration," p. 101748, 2022.

[17] A. Cipitria *et al.*, "Porous scaffold architecture guides tissue formation," vol. 27, no. 6, pp. 1275-1288, 2012.

[18] X. Bai, M. Gao, S. Syed, J. Zhuang, X. Xu, and X.-Q. J. B. m. Zhang, "Bioactive hydrogels for bone regeneration," vol. 3, no. 4, pp. 401-417, 2018.

[19] O. Tao *et al.*, "The applications of 3D printing for craniofacial tissue engineering," vol. 10, no. 7, p. 480, 2019.

[20] R. F. Pereira and P. J. J. J. o. A. P. S. Bártolo, "3D bioprinting of photocrosslinkable hydrogel constructs," vol. 132, no. 48, 2015.

[21] K. Hölzl, S. Lin, L. Tytgat, S. Van Vlierberghe, L. Gu, and A. J. B. Ovsianikov, "Bioink properties before, during and after 3D bioprinting," vol. 8, no. 3, p. 032002, 2016.

[22] Y. S. Zhang *et al.*, "3D extrusion bioprinting," vol. 1, no. 1, p. 75, 2021.

[23] X. Li *et al.*, "Inkjet bioprinting of biomaterials," vol. 120, no. 19, pp. 10793-10833, 2020.

[24] J. Malda *et al.*, "25th anniversary article: engineering hydrogels for biofabrication," vol. 25, no. 36, pp. 5011-5028, 2013.

[25] B. A. Aguado, W. Mulyasasmita, J. Su, K. J. Lampe, and S. C. J. T. E. P. A. Heilshorn, "Improving viability of stem cells during syringe needle flow through the design of hydrogel cell carriers," vol. 18, no. 7-8, pp. 806-815, 2012.

[26] D. Chimene, R. Kaunas, and A. K. J. A. m. Gaharwar, "Hydrogel bioink reinforcement for additive manufacturing: a focused review of emerging strategies," vol. 32, no. 1, p. 1902026, 2020.

[27] A. Panwar and L. P. J. M. Tan, "Current status of bioinks for micro-extrusion-based 3D bioprinting," vol. 21, no. 6, p. 685, 2016.

[28] S. Boularaoui, G. Al Hussein, K. A. Khan, N. Christoforou, and C. J. B. Stefanini, "An overview of extrusion-based bioprinting with a focus on induced shear stress and its effect on cell viability," vol. 20, p. e00093, 2020.

[29] A. GhavamiNejad, N. Ashammakhi, X. Y. Wu, and A. J. S. Khademhosseini, "Crosslinking strategies for 3D bioprinting of polymeric hydrogels," vol. 16, no. 35, p. 2002931, 2020.

[30] X. Xue, Y. Hu, S. Wang, X. Chen, Y. Jiang, and J. J. B. m. Su, "Fabrication of physical and chemical crosslinked hydrogels for bone tissue engineering," vol. 12, pp. 327-339, 2022.

[31] F. Yu, P. Yang, Z. Yang, X. Zhang, and J. J. C. E. J. Ma, "Double-network hydrogel adsorbents for environmental applications," vol. 426, p. 131900, 2021.

[32] X. Xue, Y. Hu, Y. Deng, and J. J. A. F. M. Su, "Recent advances in design of functional biocompatible hydrogels for bone tissue engineering," vol. 31, no. 19, p. 2009432, 2021.

[33] W. Hu, Z. Wang, Y. Xiao, S. Zhang, and J. J. B. s. Wang, "Advances in crosslinking strategies of biomedical hydrogels," vol. 7, no. 3, pp. 843-855, 2019.

[34] C. K. Kuo and P. X. J. B. Ma, "Ionically crosslinked alginate hydrogels as scaffolds for tissue engineering: Part 1. Structure, gelation rate and mechanical properties," vol. 22, no. 6, pp. 511-521, 2001.

[35] H. J. Yoon *et al.*, "Cold water fish gelatin methacryloyl hydrogel for tissue engineering application," vol. 11, no. 10, p. e0163902, 2016.

[36] E. Axpe and M. L. J. I. j. o. m. s. Oyen, "Applications of alginate-based bioinks in 3D bioprinting," vol. 17, no. 12, p. 1976, 2016.

[37] L. Cheng *et al.*, "Properties of an alginate-gelatin-based bioink and its potential impact on cell migration, proliferation, and differentiation," vol. 135, pp. 1107-1113, 2019.

[38] M. Sun, X. Sun, Z. Wang, S. Guo, G. Yu, and H. J. P. Yang, "Synthesis and properties of gelatin methacryloyl (GelMA) hydrogels and their recent applications in load-bearing tissue," vol. 10, no. 11, p. 1290, 2018.

[39] S. Naficy, S. Kawakami, S. Sadegholvaad, M. Wakisaka, and G. M. J. J. o. A. P. S. Spinks, "Mechanical properties of interpenetrating polymer network hydrogels based on

hybrid ionically and covalently crosslinked networks," vol. 130, no. 4, pp. 2504-2513, 2013.

[40] A. Bensimon-Brito, J. Cardeira, G. Dionísio, A. Huysseune, M. Cancela, and P. J. B. d. b. Witten, "Revisiting in vivo staining with alizarin red S-a valuable approach to analyse zebrafish skeletal mineralization during development and regeneration," vol. 16, pp. 1-10, 2016.

[41] R. D. Cardiff, C. H. Miller, and R. J. J. C. S. H. P. Munn, "Manual hematoxylin and eosin staining of mouse tissue sections," vol. 2014, no. 6, p. pdb. prot073411, 2014.

[42] A.-M. Galow *et al.*, "Increased osteoblast viability at alkaline pH in vitro provides a new perspective on bone regeneration," vol. 10, pp. 17-25, 2017.

[43] Y. Qin, L. Wang, Z. Gao, G. Chen, and C. J. S. r. Zhang, "Bone marrow stromal/stem cell-derived extracellular vesicles regulate osteoblast activity and differentiation in vitro and promote bone regeneration in vivo," vol. 6, no. 1, p. 21961, 2016.

[44] Y.-W. Chen *et al.*, "Osteogenic and angiogenic potentials of the cell-laden hydrogel/mussel-inspired calcium silicate complex hierarchical porous scaffold fabricated by 3D bioprinting," vol. 91, pp. 679-687, 2018.

[45] S. Abdulghani and G. R. J. B. Mitchell, "Biomaterials for in situ tissue regeneration: A review," vol. 9, no. 11, p. 750, 2019.

[46] D. Mao *et al.*, "Fabrication of 3D porous poly (lactic acid)-based composite scaffolds with tunable biodegradation for bone tissue engineering," vol. 142, pp. 1-10, 2018.

[47] A. C. Hernández-González, L. Téllez-Jurado, and L. M. J. C. p. Rodríguez-Lorenzo, "Alginate hydrogels for bone tissue engineering, from injectables to bioprinting: A review," vol. 229, p. 115514, 2020.

[48] A. G. Tabriz, M. A. Hermida, N. R. Leslie, and W. J. B. Shu, "Three-dimensional bioprinting of complex cell laden alginate hydrogel structures," vol. 7, no. 4, p. 045012, 2015.

[49] T. Lam *et al.*, "Photopolymerizable gelatin and hyaluronic acid for stereolithographic 3D bioprinting of tissue-engineered cartilage," vol. 107, no. 8, pp. 2649-2657, 2019.

[50] A. B. Kakarla, I. Turek, C. Kong, H. J. M. Irving, and Design, "Printable gelatin, alginate and boron nitride nanotubes hydrogel-based ink for 3D bioprinting and tissue engineering applications," vol. 213, p. 110362, 2022.

[51] Y. P. Singh, A. Bandyopadhyay, B. B. J. A. a. m. Mandal, and interfaces, "3D bioprinting using cross-linker-free silk–gelatin bioink for cartilage tissue engineering," vol. 11, no. 37, pp. 33684-33696, 2019.

[52] M. B. Łabowska, K. Cierluk, A. M. Jankowska, J. Kulbacka, J. Detyna, and I. J. M. Michalak, "A review on the adaption of alginate-gelatin hydrogels for 3D cultures and bioprinting," vol. 14, no. 4, p. 858, 2021.

[53] S. Xiao *et al.*, "Gelatin methacrylate (GelMA)-based hydrogels for cell transplantation: an effective strategy for tissue engineering," vol. 15, no. 5, pp. 664-679, 2019.

[54] C. G. Williams, A. N. Malik, T. K. Kim, P. N. Manson, and J. H. J. B. Elisseeff, "Variable cytocompatibility of six cell lines with photoinitiators used for polymerizing hydrogels and cell encapsulation," vol. 26, no. 11, pp. 1211-1218, 2005.

[55] J.-H. Wang *et al.*, "An injectable, dual crosslinkable hybrid pectin methacrylate (PECMA)/gelatin methacryloyl (GelMA) hydrogel for skin hemostasis applications," vol. 185, pp. 441-450, 2021.

[56] R. Anand, N. Nimi, V. Sivadas, L. M. R. Lal, and P. D. J. B. M. Nair, "Dual crosslinked pullulan–gelatin cryogel scaffold for chondrocyte-mediated cartilage repair: synthesis, characterization and in vitro evaluation," vol. 17, no. 1, p. 015001, 2021.

[57] J. Yin, M. Yan, Y. Wang, J. Fu, H. J. A. a. m. Suo, and interfaces, "3D bioprinting of low-concentration cell-laden gelatin methacrylate (GelMA) bioinks with a two-step cross-linking strategy," vol. 10, no. 8, pp. 6849-6857, 2018.

[58] N. Celikkin, S. Mastrogiacomo, X. F. Walboomers, and W. J. P. Swieszkowski, "Enhancing X-ray attenuation of 3D printed gelatin methacrylate (GelMA) hydrogels utilizing gold nanoparticles for bone tissue engineering applications," vol. 11, no. 2, p. 367, 2019.

[59] S. Wüst, M. E. Godla, R. Müller, and S. J. A. b. Hofmann, "Tunable hydrogel composite with two-step processing in combination with innovative hardware upgrade for cell-based three-dimensional bioprinting," vol. 10, no. 2, pp. 630-640, 2014.

[60] X. Zhou *et al.*, "3D bioprinting a cell-laden bone matrix for breast cancer metastasis study," vol. 8, no. 44, pp. 30017-30026, 2016.

[61] J. Yang *et al.*, "Localized delivery of FTY-720 from 3D printed cell-laden gelatin/silk fibroin composite scaffolds for enhanced vascularized bone regeneration," vol. 3, pp. 217-229, 2022.

[62] C. McBeth, J. Lauer, M. Ottersbach, J. Campbell, A. Sharon, and A. F. J. B. Sauer-Budge, "3D bioprinting of GelMA scaffolds triggers mineral deposition by primary human osteoblasts," vol. 9, no. 1, p. 015009, 2017.

[63] B. W. de Wildt, S. Ansari, N. A. Sommerdijk, K. Ito, A. Akiva, and S. J. C. o. i. b. e. Hofmann, "From bone regeneration to three-dimensional in vitro models: tissue engineering of organized bone extracellular matrix," vol. 10, pp. 107-115, 2019.

[64] J. Zhang *et al.*, "Optimization of mechanical stiffness and cell density of 3D bioprinted cell-laden scaffolds improves extracellular matrix mineralization and cellular organization for bone tissue engineering," vol. 114, pp. 307-322, 2020.

[65] S. Kawai *et al.*, "In vitro bone-like nodules generated from patient-derived iPSCs recapitulate pathological bone phenotypes," vol. 3, no. 7, pp. 558-570, 2019.

[66] A. Pavek *et al.*, "Tissue Engineering Through 3D Bioprinting to Recreate and Study Bone Disease," vol. 9, no. 5, p. 551, 2021.

[67] D. Loessner *et al.*, "Functionalization, preparation and use of cell-laden gelatin methacryloyl–based hydrogels as modular tissue culture platforms," vol. 11, no. 4, pp. 727-746, 2016.

[68] C. Claaßen *et al.*, "Quantification of substitution of gelatin methacryloyl: best practice and current pitfalls," vol. 19, no. 1, pp. 42-52, 2018.

[69] S. Sharifi, H. Sharifi, A. Akbari, and J. J. S. R. Chodosh, "Systematic optimization of visible light-induced crosslinking conditions of gelatin methacryloyl (GelMA)," vol. 11, no. 1, p. 23276, 2021.

[70] S. M. Siadat, D. E. Zamboulis, C. T. Thorpe, J. W. Ruberti, and B. K. J. P. i. H. S. C. T. D. Connizzo, "Tendon extracellular matrix assembly, maintenance and dysregulation throughout life," pp. 45-103, 2021.

[71] S. Yi *et al.*, "Micropore-forming gelatin methacryloyl (GelMA) bioink toolbox 2.0: Designable tunability and adaptability for 3D bioprinting applications," vol. 18, no. 25, p. 2106357, 2022.

[72] L. S. Baptista *et al.*, "Adult stem cells spheroids to optimize cell colonization in scaffolds for cartilage and bone tissue engineering," vol. 19, no. 5, p. 1285, 2018.

[73] A. Blaeser, D. F. Duarte Campos, U. Puster, W. Richtering, M. M. Stevens, and H. J. A. h. m. Fischer, "Controlling shear stress in 3D bioprinting is a key factor to balance printing resolution and stem cell integrity," vol. 5, no. 3, pp. 326-333, 2016.

[74] T. Jain *et al.*, "Impact of cell density on the bioprinting of gelatin methacrylate (GelMA) bioinks," vol. 22, p. e00131, 2021.

[75] C. B. Khatiwala, S. R. Peyton, and A. J. J. A. J. o. P.-C. P. Putnam, "Intrinsic mechanical properties of the extracellular matrix affect the behavior of pre-osteoblastic MC3T3-E1 cells," vol. 290, no. 6, pp. C1640-C1650, 2006.